Nanostructured surface for extended temperature operating range in concentrator photovoltaic modules

Gavin Forcade, Christopher E Valdivia, Philippe St-Pierre, Arnaud Ritou, Ma té Volatier, Abdelatif Jaouad, Maxime Darnon, Karin Hinzer

Nanostructured Surface for Extended Temperature Operating Range in Concentrator Photovoltaic Modules

Gavin Forcade[1, a)], Christopher E. Valdivia[1], Philippe St-Pierre[2], Arnaud Ritou[2], Maïté Volatier[2], Abdelatif Jaouad[2], Maxime Darnon[2], and Karin Hinzer[1]

[1]*SUNLAB, Centre for Research in Photonics, University of Ottawa, Ottawa, On, Canada.*
[2]*Laboratoire Nanotechnologies et Nanosystèmes, LN2, CNRS, Université de Sherbrooke, Institut Interdisciplinaire d'Innovation Technologique (3IT), QC, Canada.*

[a)] Corresponding author: gforc034@uottawa.ca

Abstract. Concentrator photovoltaic (CPV) systems that use silicone-on-glass Fresnel lenses as their primary optical element have reduced power output at high and low lens temperatures. We show that incorporating a nanostructured surface on the solar cell stabilizes best module performance over an extended operating temperature range. We model the optical properties of a self-organized monolayer of glass beads deposited on a polydimethylsiloxane (PDMS) encapsulated solar cell in a CPV sub-module. Our model combines transfer matrix method (TMM), rigorous coupled wave analysis (RCWA), and ray tracing to quickly and accurately simulate the system. We find the short-circuit current gain increases as the lens deviates from its designed working temperature for all bead sizes, and that 400 nm diameter beads submerged halfway into PMDS have the highest gain (up to 2.6%).

INTRODUCTION

III-V photovoltaic cells have the highest conversion efficiency of sunlight to electrical energy, up to 47.1% under concentrated light [1]. However, high costs limit their applications to space where high power-to-weight ratio dominates over device cost [2]. Advances in cost, efficiency, and energy collection are required for wider adoption of these devices within terrestrial concentrator photovoltaic (CPV) systems. CPV modules use relatively inexpensive optics to concentrate sunlight by hundreds of times onto solar cells, demonstrating the highest module efficiency of 36.7% [3] and, with a highly transmissive lens, a sub-module efficiency of 43.4% [4]. CPV has the potential to provide energy at both high yields and low costs for locations with a high solar resource [5] but must compete with the low cost of conventional non-concentrating Si photovoltaic (PV) panels [6]. Silicone-on-glass (SoG) Fresnel lenses provide an inexpensive yet high-performance platform for solar concentration but suffer from temperature-related focusing errors, illustrated in Fig. 1. These focussing errors result from two orders of magnitude difference between the coefficients of thermal expansion of silicone and glass, and from the temperature-dependent refractive indices [7]. These effects reduce the annual energy yield of CPV systems, reaching a calculated 8% absolute reduction for regions with large temperature variations [8]. Curing the silicone at the lens operating temperature minimizes the focusing errors [9] but customizing modules for regional deployment greatly increases manufacturing costs. Instead, Hornung et al. [10] numerically optimized the SoG Fresnel lens structure to lower the thermally-varying optical efficiency from 11.6% to 3.1% (absolute) for lens temperatures from 10 to 60ºC. Performance can be further improved by placing a secondary optical element (SOE) on the solar cell [11] but adds cost and complexity to CPV modules.

The approach present herein employs a relatively inexpensive nanostructured surface on the solar cell to improve the temperature-dependent performance of the CPV system. Nanostructured surfaces can increase the transmission of light into the solar cell relative to flat surfaces by providing a smoothly-varying effective refractive index transition [12]. Researchers at CEA-LITEN (France) developed a colloidal dynamic fluid-flow process to create a micro- or nano-structured surface by depositing a self-organized monolayer of glass or silica beads on a polydimethylsiloxane

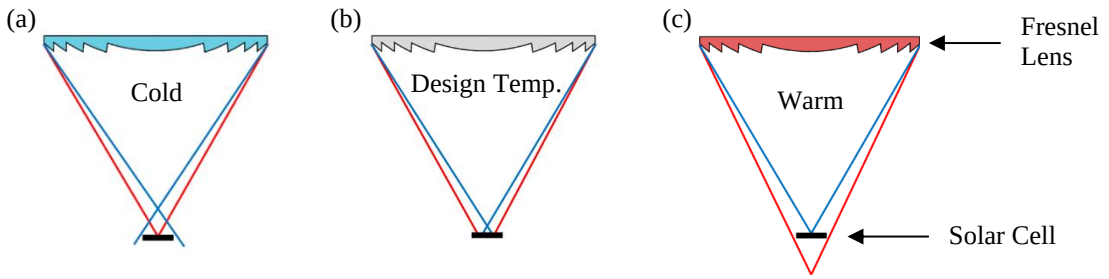

FIGURE 1. The modeled CPV sub-module (incorporating the SoG Fresnel lens and solar cell), illustrating the temperature-dependent focusing accuracy of a: (a) cold lens; (b) lens at its design temperature; and (c) warm lens. The blue and red lines represent short and long wavelengths, respectively.

(PDMS) layer [13]. We employ an optical model to explore the benefits of beads deposited on a PDMS-encapsulated triple-junction solar cell (3JSC) in a CPV sub-module. We optimize the bead size, its submergence depth into PDMS, and the PDMS layer thickness to maximize the system's short-circuit current. We find the highest current gain for 400 nm diameter beads submerged halfway into a 5 μm PDMS layer. We also show the beads reduce the impact of SoG Fresnel lenses varying from their design temperature.

MATERIALS AND METHODS

Optical Model Description

Our model simulates the optical behavior of a CPV sub-module, combining transfer matrix method (TMM), rigorous coupled wave analysis (RCWA), and ray tracing, as shown in Fig. 2(a,b). We apply an open-source TMM code [14] to simulate the optical behavior of the 3JSC, providing the external and internal reflections, transmissions and absorptions throughout the multi-layer stack. Since we did not know the exact design of the 3JSC, the parameters used in TMM were extracted from fits to measured reflection data of the 3JSC. To accurately simulate the optical effects of the sub-wavelength structure formed by the bead monolayer, we apply an open-source RCWA code, RETICOLO [15], which provides wavelength- and angle-resolved transmission, reflection, and scattering for the air-bead-PDMS interface. The results of both simulations are inserted as boundary conditions into the commercial ray tracing software, Zemax, allowing it to correctly simulate the optical properties of the entire sub-module [16], including the 3JSC stack and the sub-wavelength structures of the bead monolayer. The resulting angle dependent irradiance profile on the 3JSC for the CPV sub-module is shown in Fig. 2(c).

To model the temperature-dependent performance of the SoG Fresnel lens, we relate its temperature to a focal length using a linear coefficient (0.107 mm/°C) extracted from data measured over a temperature range of 25-50ºC [7]. To model a wider operational range, we applied the same coefficient for lens temperatures down to -25ºC.

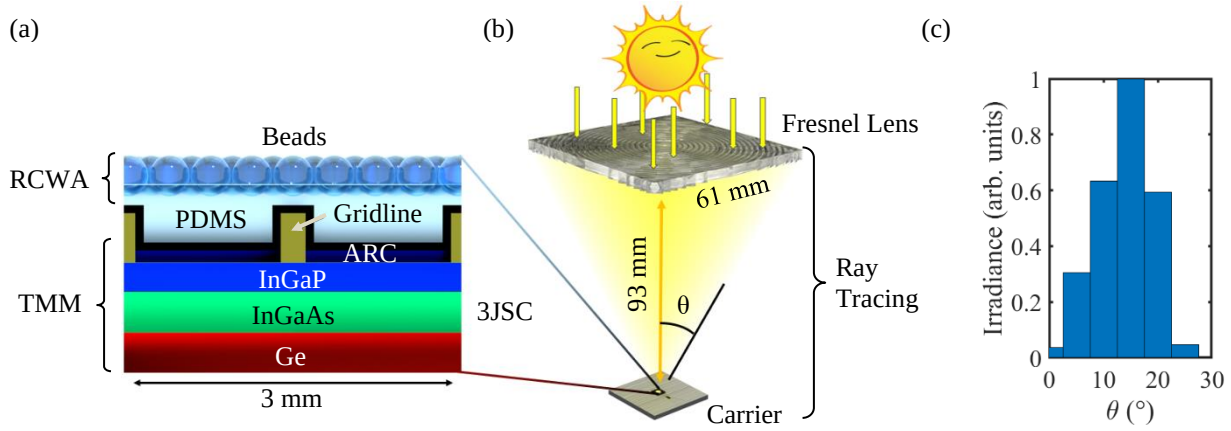

FIGURE 2. Illustration of the sections modeled by each optical software: (a) cross-sectional view of the PDMS-encapsulated 3JSC (TMM) with a micro-bead top surface (RCWA); and (b) CPV sub-module (ray tracing). (c) Irradiance profile on the 3JSC.

Optimization Procedure

To quantify the improved transmission of light through the air-bead-PDMS interface, we calculate the spectrum-weighted transmission for the i^{th} subcell as follows:

$$T_{\text{W},i} = \int T_{\text{PDMS}}(\lambda) \frac{Irr_{\text{AM1.5D}}(\lambda)}{E_{\text{ph}}(\lambda)} IQE_i(\lambda)\, d\lambda \tag{1}$$

where λ is the wavelength of light, T_{PDMS} is the transmission from air through the beads and into the PDMS (see Fig. 4(a)), $Irr_{\text{AM1.5D}}$ is the ASTM G173-03 direct-beam spectral irradiance, E_{ph} is the photon energy, and IQE_i is the internal quantum efficiency of the i^{th} subcell, shown in Fig. 3. Experimental measurements validated that the IQE_i is constant for all incident angles of light encountered by the solar cell. Also, we assume the IQE_i is constant with cell temperature.

We find the optimal bead size by maximizing the short-circuit current of the solar cell. Since the 3JSC is made of 3 series-connected subcells, we calculate its short circuit current by taking the minimum of the subcell currents:

$$I_{\text{sc}} = \min\left(q \int \frac{Irr_{\text{AM1.5D}}(\lambda)}{E_{\text{ph}}(\lambda)} T_{\text{Total}}(\lambda)\, IQE_i(\lambda)\, d\lambda\right) \tag{2}$$

where q is the electronic charge, and T_{Total} is the total transmission from the SoG Fresnel lens through the PDMS and into the 3JSC. To quantify the impact of incorporating beads in our system, we investigate the gain of both the weighted transmission through the PDMS layer and the 3JSC short-circuit current as follows:

$$T_{\text{W},i}^{\text{gain}} = \left(\frac{T_{\text{W},i}^{\text{Beads}}}{T_{\text{W},i}^{\text{noBeads}}} - 1\right) \tag{3}$$

$$I_{\text{sc}}^{\text{gain}} = \left(\frac{I_{\text{sc}}^{\text{Beads}}}{I_{\text{sc}}^{\text{noBeads}}} - 1\right) \tag{4}$$

where $T_{\text{W},i}^{\text{Beads}}$, $I_{\text{sc}}^{\text{Beads}}$ and $T_{\text{W},i}^{\text{noBeads}}$, $I_{\text{sc}}^{\text{noBeads}}$ are calculated with and without beads, respectively.

RESULTS AND DISCUSSION

Optical Performance at the Air-Bead-PDMS Interface

Figure 3 shows the transmission of perpendicularly incident light (relative to the solar cell) through the air-bead-PDMS interface as a function of wavelength for beads submerged halfway into PDMS. The 280 nm beads have a

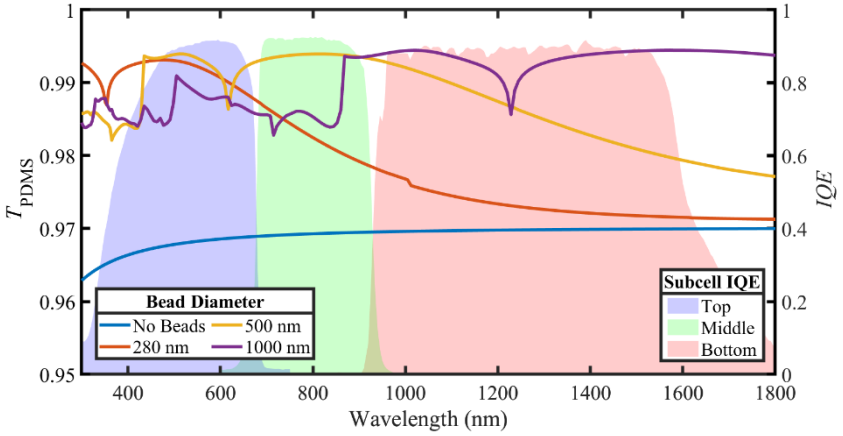

FIGURE 3. (Left-axis) Transmission of perpendicularly incident light through the air-bead-PDMS interface for beads submerged halfway into PDMS. (Right-axis) The measured internal quantum efficiency of the 3JSC used in our model.

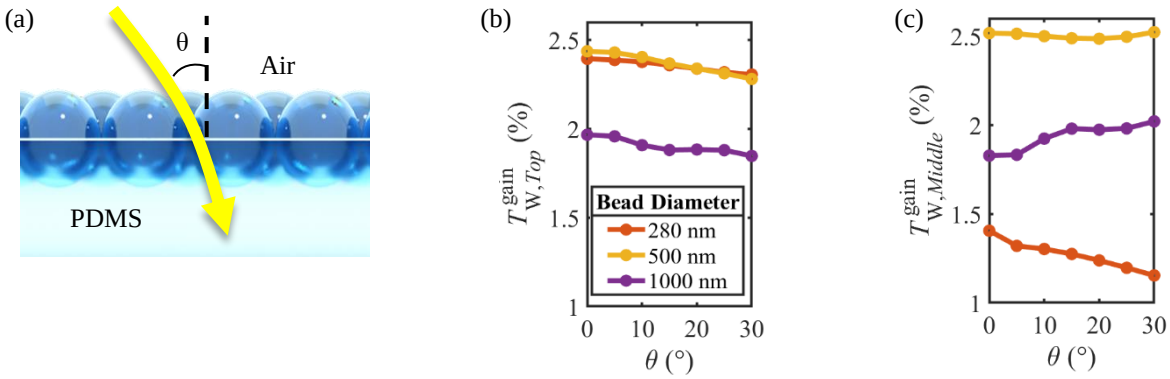

FIGURE 4. (a) Illustration of angled light transmitting through the air-bead-PDMS interface. The graphs show the spectrum-weighted transmission gai for beads submerged halfway into PDMS as a function of the incident angle of light relative to the PDMS surface normal for the (b) top subcell and (c) middle subcell.

relatively low transmission for long wavelengths because of the short transition distance for the effective refractive index relative to the wavelength size. The 1000 nm beads transmit less and has a rough profile at smaller wavelengths because the interaction regime changes from smoothly-varying effective refractive index to diffraction. Therefore, the highest overall transmission of wavelengths absorbed in the top 2 subcells is close to 500 nm.

Both Figures 4 and 5 present the spectrum-weighted transmission through the air-bead-PDMS interface for wavelengths absorbed within the top 2 subcells, ignoring the bottom subcell since we found it never limits the current for all the simulated conditions. Figure 4 depicts the transmission of light as a function of its angle of incidence relative to the cell surface normal. First, notice that transmission improves for all incident angles and bead sizes explored. Second, the transmission gain stays relatively stable for the angles of incidence shown. Finally, 500 nm beads have the highest overall transmission of wavelengths absorbed by the top 2 subcells, in agreement with results from Fig. 3.

Figure 5 depicts the transmission gain for beads submerged at various depths into PDMS. As can be seen, beads should be submerged at least 20% into PDMS and show optimal performance near ~50%. This behavior can be explained by the effective refractive index profile as the bead submergence is varied. Beads submerged less than halfway into PDMS yield an effective refractive index profile that transitions back towards air below the bead center. Conversely, beads submerged further than 50% into PDMS increase the abruptness of the effective refractive index transition at the PDMS surface.

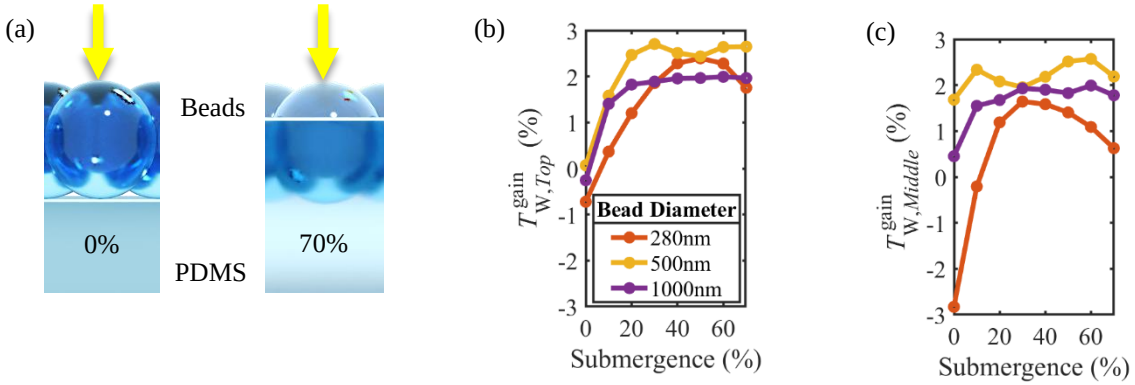

FIGURE 5. (a) Illustration of beads 0% and 70% submerged into PDMS. The graphs show the spectrum-weighted transmission gain for light perpendicularly incident to the PDMS surface with beads submerged at various depths into the PDMS for the (b) top subcell and (c) middle subcell.

Performance of CPV Sub-Modules with Beads

We now present simulation results of the complete CPV sub-module, with beads submerged halfway into the PDMS. Figure 6(a) shows the short-circuit current of the 3JSC for a range of lens temperatures. We calculate a higher and flatter current response for all bead sizes relative to no beads. Current curve flattening is largest at ~10ºC for

280 nm beads. The currents produced for a lens temperature of 10ºC versus the temperature producing the maximum current (30ºC) is 1.3% lower for 280 nm beads compared to 2.4% lower for no beads.

Figure 6(b) shows the short-circuit current gain of the 3JSC for a range of lens temperatures. Firstly, these calculations show an improved current generation for all conditions in comparison to the performance without beads. Secondly, the current gain improves for both a warmer and colder lens relative to the 30ºC designed temperature. As the lens temperature increases from 25ºC, longer wavelengths increasingly miss the 3JSC (see Fig. 1), transitioning to a current limited by the middle subcell. Under high temperatures, small beads better transmit this red-deficient spectrum (see 280 nm beads in Fig. 3) and reduced range of incident angles (see Fig. 4(c)), thus yielding an improved current gain. Conversely, as the lens temperature dips below 25ºC, short wavelengths increasingly miss the 3JSC (see Fig. 1), operating with a current-limiting top subcell. Under low temperatures, large beads better transmit the blue-deficient spectrum (see 1000 nm beads in Fig. 3) which improves the current gain. The two scenarios provide support to incorporate beads into our modeled CPV sub-module to improve its temperature-dependent short-circuit current output. Finally, Fig. 6(b) shows the largest current gain (2.6%) is reached at a -25ºC lens for 400 nm beads because they provide the highest transmission for wavelengths absorbed by the top limiting subcell. However, the best average performance is reached by ~500 nm beads, since they have the highest overall transmission within the absorption range of both limiting subcells.

Figure 6(c) presents the effects of PDMS layer thickness on the short-circuit current of the CPV sub-module. The blue curves show the current gain for a PDMS layer that is thicker than 5 μm, without the incorporation of beads. As shown, a thicker PDMS layer improves the short-circuit current gain of cold lenses but suffers a small loss for warm lenses. The relatively large improvement of ~0.8% at -25ºC is due to a combination of a low starting point efficiency and that all rays that hit the PDMS top surface reach the solar cell. The red curves show the current gain from incorporating 400 nm beads, submerged halfway in PDMS. Hot lenses have improved short-circuit current gains for thicker PDMS layers, because longer wavelengths increasingly miss the PDMS top surface (see Fig. 1(c)) and 400 nm beads better transmit this red-deficient spectrum.

Our model does not consider the absorption in PDMS, and since the improvement from having a thicker PDMS layer is relatively small it is likely that the best thickness is closer to ~5 μm. Finally, both Fig. 6(b,c) have a large jump at a lens temperature of ~15ºC because the current limiting subcell switches. The jump is less prominent for large beads since they improve the current relatively equally for both subcells.

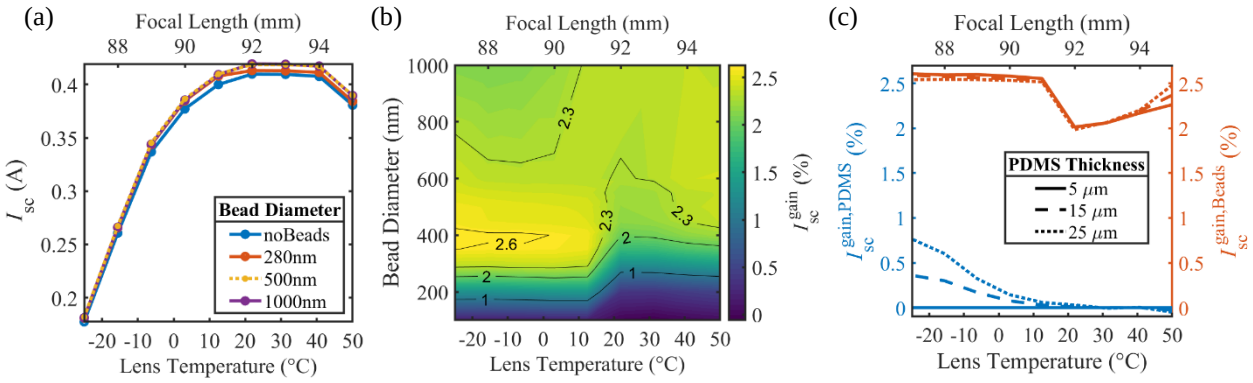

FIGURE 6. Short-circuit current, (a) absolute and (b,c) gain, of our modeled CPV sub-module as a function of lens temperature. (a,b) Compares effects of bead sizes on current. (c) Blue lines compare thicker layers to a 5 μm PDMS layer, all without beads; red lines compare gains when adding 400 nm beads on PDMS layers of differing thickness.

CONCLUSION

We modeled the optical behavior of a CPV sub-module with a nanostructured surface on a PDMS-encapsulated III-V 3JSC. The nanostructured surface consists of a deposited self-organized monolayer of silica beads that sink into PDMS. Sunlight perceives an effective refractive index that smoothly changes from air to PDMS which improves its transmission. We find the PDMS layer thickness does not have a significant impact on the short-circuit current of the system, thus its thickness should be designed with respect to other aspects not considered here, such as absorption. We find the nanostructured surface improves the sub-module's current output by reducing its temperature dependence.

Also, 400 nm beads submerged halfway into PDMS has the highest short-circuit current gain up to ~2.6%, but ~500 nm beads have a better overall performance over the full temperature range explored.

ACKNOWLEDGMENTS

We acknowledge the support from STACE, the Quebec Ministry of Economy and Innovation, MITACS, CMC microsystems, NSERC, and the Ontario Research Fund. The support from CEA-LITEN is also acknowledged. LN2 is a joint International Research Laboratory (Unité Mixte Internationale UMI 3463) funded and co-operated in Canada by Université de Sherbrooke (UdeS) and in France by CNRS as well as Université de Lyon (UdL , especially including ECL, INSA Lyon, CPE) and Université Grenoble Alpes (UGA). It is also associated to the French national nanofabrication network RENATECH and is supported by the Fonds de Recherche du Québec Nature et Technologie (FRQNT).

REFERENCES

1. J. F. Geisz, R. M. France, K. L. Schulte, M. A. Steiner, A. G. Norman, H. L. Guthrey, M. R. Young, T. Song, and T. Moriarty, "Six-junction III–V solar cells with 47.1% conversion efficiency under 143 Suns concentration," *Nature Energy* **5**, 326–335 (2020).
2. X. Q. Liu, C. Fetzer, P. Chiu, M. Haddad, X. Zhang, R. Cravens, D. Law, J. Ermer, J. Krogen, S. Sharma, and J. Hanley, "Large Area Multijunction III-V Space Solar Cells Over 31% Efficiency," *44th Photovoltaic Specialist Conference (PVSC)*, 2094-2098 (2017).
3. M. Steiner, A. Bosch, A. Dilger, F. Dimroth, T. Dorsam, M. Muller, T. Hornung, G. Siefer, M. Wiesenfarth, and A. Bett, "FLATCON CPV module with 36.7% efficiency equipped with four-junction solar cells," *Progress in Photovoltaics: Research and Applications* **23**, 1323-1329 (2015).
4. M. Steiner, G. Siefer, T. Schmidt, M. Wiesenfarth, F. Dimroth, and A. W. Bett, "43% Sunlight to electricity conversion efficiency using CPV," *Journal of Photovoltaics* **6**, 1020-1024 (2016).
5. E. F. Fernandez, D. L. Talavera, F. M. Almonacid, and G. P. Smestad, "Investigating the impact of weather variables on the energy yield and cost of energy of grid-connected solar concentrator systems," *Energy* **106**, 790-801 (2016).
6. K. A. W. Horowitz, M. Woodhouse, H. Lee, and G. P. Smestad, "A bottom-up cost analysis of a high concentration PV module," *11th International Conference on Cncentrator Photovoltaic Systems* **1679**, 100001 (2015).
7. V. D. Rumyantsev, N. Y. Davidyuk, E. A. Ionova, and V. M. Andreev, "Thermal regimes of Fresnel lenses and cells in all glass HCPV modules," *6th International Conference on Concentrator Photovoltaic Systems* **1277**, (2010).
8. T. Hornung, M. Steiner and P. Nitz, "Estimation of the influence of Fresnel lens temperature on energy generation of a concentrator photovoltaic system," *Solar Energy Materials & Solar Cells* ***99***, 333 - 338 (2012).
9. S. Askins, M. Victoria, R. Herrero, C. Dominguez, I. Anton, and G. Sala, "Effects of temperature on hybrid lens performance," 7*th International Conference on Concentrator Photovoltaic Systems* **1407**, 57 (2011).
10. T. Hornung, M. Neubauer, A. Gombert, and P. Nitz, "Fresnel lens concentrator with improved thermal behavior," 7*th International Conference on Concentrator Photovoltaic Systems* **1407**, 66 (2011).
11. S. Askins, M. Perez, R. Gerrero, C. Dominguez, I. Anton, A. Coutinho, and J. Amador, "Optimizing CPV systems for thermal and spectral tolerance," *27th European Photovoltaic Solar Energy Conference and Exhibition*, 194 – 198 (2012).
12. W. Wang and A. Freundlich, "Simulation and development of sub-wavelength grated dielectric ARCs for CPV applications," *39th Photovoltaic Specialists Conference*, 3049-3052 (2013).
13. P. Garcia-Linares, C. Dominguez, O. Dellea, T. Kampfe, Y. Hourlin, P. Besson, C. Weick, and M. Baudrit, "Improving optical performance of concentrator cells by means of a deposited nanopattern layer," *11th International Conference on Concentrator Photovoltaic Systems* **1679**, 40004 (2015).
14. S. J. Byrnes, "Multilayer optical calculations," arXiv: 1603.02720 (2016).
15. J. P. Hugonin and P. Lalanne, "RETICOLO software for grating analysis," Institut d'Optique. Orsay, France (2005).
16. P. Sharma, M. M. Wilkins, H. P. Schriemer, and K. Hinzer, "Concentrating optical system optimization for 3- and 4-junction solar cells: impact of illumination profiles," *J. Photon. Energy* **7**(**1**), 014501 (2017).